Retrieval of the precipitable water vapor from shipborne multi-GNSS measurements in tropical cyclone-prone regions of the Northwest Pacific during the summer season in 2021

Dong-Hyo Sohn[1], Byung-Kyu Choi[1], Junseok Hong[1], Yosup Park[2], Hwimin Jang[3], Byung-Il Lee[4], Jong-Kyun Chung[1]

[1]Center for Space Navigation & Geodesy, Division of Space Information Research, Korea Astronomy and Space Science Institute, Daejeon 34055, Republic of Korea
[2]Maritime Robotics Test & Evaluation Center, Marine Industry Research Division, Korea Institute of Ocean Science and Technology, Busan 49111, Republic of Korea
[3]Vessel Observation Team, Vessel Management Department, Korea Institute of Ocean Science and Technology, Busan 49111, Republic of Korea
[4]Satellite Analysis Division, National Meteorological Satellite Center, Jincheon-gun, Chungcheongbuk-do 27803, Republic of Korea

Correspondence to: Dong-Hyo Sohn (dhsohn@kasi.re.kr)

Abstract. Global Navigation Satellite System (GNSS) is useful for monitoring atmospheric precipitable water vapor (PWV) content. GNSS observations performed in the ocean are relatively rare, making PWV observations at sea difficult to achieve. We previously retrieved shipborne GNSS PWV in the Northwest Pacific and conducted a comparative study with other observation systems. In this study, we demonstrate that reliable results can be obtained for the shipborne GNSS PWV over the ocean by using observations from similar regions at different times and comparing them with another dataset. To achieve this, we introduce the retrieval and validation of PWV from shipborne GNSS observations conducted aboard the research vessel from July 30 to August 25, 2021, in tropical cyclone-prone regions of the Northwest Pacific Ocean. The shipborne GNSS-derived PWV is validated against three reference datasets - radiosonde, low Earth orbit satellite (MetOp-IASI), and geostationary satellite (GK2A-AMI) - to assess its accuracy and reliability in oceanic environments. The GNSS PWV exhibits good agreement with radiosonde measurements, with a mean bias of −0.94 mm and a root mean square (RMS) of 4.28 mm. In addition, the GNSS PWV and radiosonde PWV exhibit a correlation coefficient of 0.80. A comparison between GNSS-derived PWV and PWV obtained from GK2A-AMI observations reveals a minimal mean bias of 0.08 mm, which indicates good agreement. The RMS value between the two datasets is slightly greater than that observed with the radiosonde, reaching 4.83 mm. This comparison yields a correlation coefficient of 0.79. Furthermore, the PWV derived from MetOp-IASI shows a substantial bias of 2.58 mm and a relatively large RMS error of 6.99 mm compared with the GNSS PWV, with a correlation coefficient of 0.71. These results are consistent with previous findings. In particular, following the development of a tropical cyclone in the Northwest Pacific, we found a strong correlation between the GNSS PWV variation and precipitation. We suggest that the PWV derived from shipborne GNSS observations in tropical cyclone-prone regions of the Northwest Pacific provides stable and reliable results.

1 Introduction

The Global Navigation Satellite System (GNSS), which includes the Global Positioning System (GPS), Global Navigation Satellite System (GLONASS), Galileo, and BeiDou, is an effective tool for estimating the signal delay caused by water vapor in the troposphere. Bevis et al. (1992) initially derived the precipitable water vapor (PWV) from the analysis of tropospheric delays in data from ground-based GPS networks. Since then, a considerable number of studies on PWV have been conducted using ground GNSS stations (Niell et al., 2001; Wang and Zhang, 2008; He and Liu, 2020). Currently, the international GNSS service (IGS) provides the highest-quality GNSS data, tropospheric products, and services with a global network of more than 500 GNSS ground stations (IGS, 2025). The vast majority of IGS stations and nationally operated GNSS stations are located on land. The land covers roughly 30 percent of the Earth's surface. Therefore, there are limitations to monitoring the overall variation in PWV on Earth using only GNSS stations on land.

In contrast, the ocean covers over 70 percent of Earth's surface. Severe meteorological phenomena such as tropical cyclones originate over the sea. Observing these phenomena requires global surveillance, but most of the GNSS equipment that receives satellite signals is installed on land. On the other hand, GNSS observation data in the ocean is relatively scarce compared to those on land due to the difficulty of maintaining fixed stations in the marine environment. GNSS observations made in the ocean are making PWV observations challenging to achieve over the sea. In general, the amount of vertically integrated water vapor above the oceans can be retrieved using a microwave radiometer on board meteorological satellites. Satellite-borne sensors have the advantage of being able to make global observations covering a wide area. However, satellite observation provides a relatively low spatial resolution. Also, Earth observation satellites have a long revisit period, the elapsed time between observations of the same point (Kealy et al., 2012; Smith et al., 2019).

Some studies have shown the potential of shipborne GNSS PWV retrieval. The shipborne GNSS-derived PWV is in good agreement with radiosonde observations, which are used as a reference to assess the measurement of atmospheric water vapor. In open oceans, shipborne GPS PWV and radiosonde measurements are shown to agree with a root mean square (RMS) of differences of 2–5 mm (Rocken et al., 2005; Fujita et al., 2008; Kealy et al., 2012; Shoji et al., 2017; Wang et al., 2019). Satellite observations are also an excellent resource for comparing observations made at sea. The produced PWV based on the satellite images provides information close to global coverage with high spatiotemporal resolution. The satellite-based sensors, such as the moderate resolution imaging spectroradiometer (Boniface et al., 2012; Bosser et al., 2021), the atmospheric infrared sounder aboard NASA's Aqua satellite (Sohn et al., 2020), and the calibration microwave radiometer on board the Haiyang-2A satellite (Liu et al., 2019; Wu et al., 2020), have shown accuracy with an RMS of less than 10 mm. The results calculated in the sea are also verified with a numerical weather model. The shipborne GNSS-derived PWV dataset is well coincident with models such as the fifth-generation Penn State/NCAR Mesoscale Model (Fan et al., 2016), the European Centre for Medium-range Weather Forecasts fifth reanalysis (Bosser et al., 2021, 2022; Männel et al., 2021; Panetier et al., 2022). It is shown to have RMS differences of less than 10 mm. In addition, the PWV observed by GNSS onboard the vessel has been assimilated

for improving the accuracy of precipitation forecasts. Ikuta et al. (2022) investigated that the assimilation of shipborne PWV observations can improve the prediction accuracy of heavy rainfall events, especially precipitation amount and location.

Water vapor is one of the important factors driving weather patterns. In particular, the water vapor evaporated from warm ocean water plays an important role in the formation and development of a tropical cyclone in the Northwest Pacific. The Korea Meteorological Administration (KMA) reported that about 87% of tropical cyclones that influenced the Korean Peninsula occurred between July and September for the period 1991–2020 (KMA, 2022). Tropical cyclones are generated in the region of approximately 110°–160°E and 5°–25°N, and some of them approach the Korean Peninsula via the Philippine Sea and the East China Sea (Park et al., 2006; He et al., 2017; JMA, 2022). Kang et al. (2024) showed that the combination of high ocean heat content of the North Equatorial Current flowing between 8°N and 17°N and low salinity-driven upper-layer stratification makes a rapid intensification of super typhoons. Therefore, high ocean heat content is strongly associated with elevated atmospheric water vapor levels.

Sohn et al. (2020) reported on the retrieval of PWV from shipborne GNSS observations in the Northwest Pacific region from August to September 2018. They calculated PWV using GPS-only data from low-cost equipment and compared it with other datasets (radiosonde and atmospheric infrared sounder on NASA's Aqua satellite). Later, another GNSS equipment with high-precision and multi-constellation capabilities was additionally installed on a vessel. This study focuses on whether a comparable and stable data quality of the shipborne GNSS PWV can be obtained over different time periods with different other PWV datasets using the additional GNSS equipment based on previous research. In particular, we aim to show that it is produced stably even in the low-latitude ocean during tropical cyclone-prone periods. The vessel operated in the Northwest Pacific region, the Philippine Sea, for a period similar to that of previous studies. We adopt the GNSS kinematic precise point positioning (PPP) method, which uses dual-frequency data obtained from multi-GNSS measurements onboard the vessel. The shipborne GNSS-derived PWV is validated against three datasets, including ship-launched radiosonde measurements and spaceborne observations from low Earth orbit and geostationary satellites. While this work is limited to analyzing PWV estimated along the track of a single vessel, it aims to demonstrate the practical usefulness and stability of PWV measurements obtained from a shipborne GNSS receiver over the ocean.

2 GNSS configurations and data processing

2.1 GNSS configurations

Shipborne GNSS PWV was estimated from multi-GNSS measurements obtained from a research vessel (R/V) ISABU. The R/V ISABU is an ocean science research vessel operated by the Korea Institute of Ocean Science and Technology (KIOST) that conducts operations in the Northwest Pacific region in the second half of every year. This vessel has an overall length of 99.8 meters, a width of 18 meters, and a total weight of 5,894 tons. Although a maritime GNSS antenna has been set up on the mast, the GNSS antenna used for monitoring atmospheric water vapor in this study is additionally installed on a vessel's foremast, as shown in Fig. 1. The measurements are logged on a Trimble NetR9 receiver connected to an Aeroantenna

Technology Inc. AT1675-7MW antenna (same model as: Magellan Professional MAG111406 antenna). The receiver offers 440 channels to track GPS, GLONASS, Galileo, and BeiDou constellations. The antenna is a high-performance, dual-frequency GNSS antenna designed for precision applications. It can acquire continuous GNSS data with a 30-second sampling interval.

R/V ISABU operated in the Northwest Pacific for scientific research during one cruise from July 30 to August 25, 2021. The vessel starts its cruise from the port on day of year (DOY) 211 (30 July), and heads southward to the Philippine Sea until DOY 214 (2 August). The marine science experiment lasted 20 days, and then the vessel headed northward until reaching port on DOY 237 (25 August).

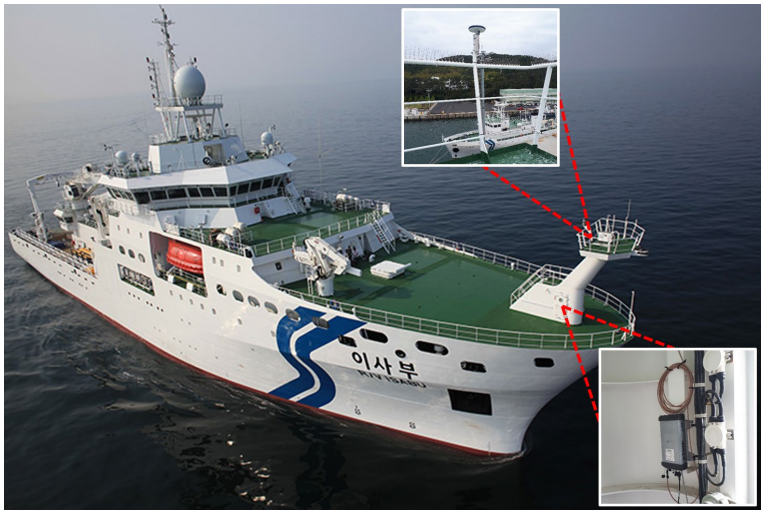

Figure 1. The global navigation satellite system (GNSS) antenna and receiver are installed on the foremast of the research vessel ISABU.

2.2 Data processing

This study employs the GNSS kinematic precise point positioning (PPP) method using dual-frequency measurements from a shipborne multi-GNSS receiver. PPP is a positioning method that provides a high level of position accuracy using a single GNSS receiver only. This method can be used to estimate the precise positioning and the amount of water vapor in the atmosphere. To perform kinematic PPP using multi-constellation GNSS, we use a multi-GNSS analysis software (MGAS) developed by the Korea Astronomy and Space Science Institute (Choi et al., 2017, 2018). MGAS is capable of supporting multiple data processing strategies, such as static, kinematic, and dynamic options. Data from a continuously moving ship processed using kinematic PPP mode.

The German research centre for geosciences (GFZ) multi-GNSS experiment (MGEX) series is employed to estimate precise ship positioning and tropospheric zenith total delay (ZTD) (Deng et al., 2016). These products include precise orbits and clock corrections for GPS, GLONASS, Galileo, and BeiDou satellites. Tropospheric delay is still a significant error source in GNSS precise positioning. In the PPP processing, the tropospheric ZTD is estimated as an unknown parameter. For ZTD calculation,

the Saastamoinen model (Saastamoinen, 1973) with global pressure and temperature 2 (GPT2) (Lagler et al., 2013) is employed as a prior value. In addition, the global mapping function (GMF) (Boehm et al., 2006) is used for tropospheric mapping.

The methods and models used in the PPP processing are summarized in Table 1. For the kinematic PPP, we used dual-frequency observations from GPS (L1/L2), GLONASS (L1/L2), Galileo (E1/E5a), and BeiDou (B1/B2). Although the shipborne GNSS observation sampling interval was 30 s, the data were resampled to 5-minute intervals for the kinematic PPP processing. Accordingly, the precise coordinates and tropospheric ZTD values were estimated every 5 minutes. Tropospheric horizontal gradients are also estimated at 5-minute intervals to compensate for atmospheric azimuthal asymmetry. These parameters are estimated as random walk processes. Due to the high correlation among coordinates, receiver clock, and troposphere in kinematic PPP, setting appropriate process noise is crucial. To accommodate the dynamic marine environment of the moving vessel, the process noise for the coordinates and receiver clocks was applied following the configuration suggested by Choi et al. (2018). The tropospheric ZTD and horizontal gradients were assigned process noises of 2.5 mm/$\sqrt{h}$ and 0.3 mm/$\sqrt{h}$, respectively (Choi et al., 2012). To maintain consistency in the processing strategy, Earth rotation parameters were derived from GFZ products. Both satellite and receiver antenna phase center offsets (PCO) and phase center variations (PCV) are corrected using the absolute IGS antenna correction file (igs14_2188.atx). The receiver clock offset is estimated as a stochastic parameter using a Gauss-Markov process. Phase wind-up effects are corrected with the method proposed by Wu et al. (1993). The ionosphere is the largest source of error in GNSS signal propagation. Ionospheric error is eliminated by the ionosphere-free linear combination of dual-frequency carrier-phase and code observations. Carrier-phase ambiguities are estimated as float values for parameter estimation.

Table 1. Models and methods for multi-GNSS kinematic PPP processing.

Item	Models and Methods
Signals	GPS (L1, L2), GLONASS (L1, L2), Galileo (E1, E5a), BeiDou (B1, B2)
Sampling rate	30 sec
Elevation cufoff	10°
Satellite orbit and clock	GFZ MGEX series
Earth rotation parameters	GFZ MGEX series
Satellite PCO/PCV	igs14_2188.atx
Receiver PCO/PCV	igs14_2188.atx
Receiver clock	Estimated by the Gauss-Markov model
Phase wind-up	Wu et al. (1993) & nominal yaw-steering mode
Ionospheric delay	Eliminated by the ionosphere-free linear combination
Tropospheric delay	Estimated with zenith wet delay, tropospheric gradient component
Tropospheric mapping function	GMF
Meteorological information	GPT2

Ambiguity	Float solutions

2.3 GNSS Precipitable water vapor (PWV) estimation

The PWV is equivalent to the volume per unit area of liquid water under standard atmosphere when all of the water vapor contained in a vertical column of air per unit cross-section from the surface of the Earth to the top of the atmosphere is condensed and precipitated.

The tropospheric delay can be separated into a dry component (zenith hydrostatic delay, ZHD) and a wet component (zenith wet delay, ZWD) (Davis et al., 1985). ZHD is assimilated to a hydrostatic model as follows:

$$ZHD = \frac{0.0022768\, P_s}{1-0.00266\cos(2\phi)-0.00028\, H} \quad (1)$$

where P_s is the total pressure at the Earth's surface in millibars, ϕ is the geodetic latitude, and H is the height of the station on the ellipsoid in kilometres (Elgered et al., 1991). Surface pressure P_s is estimated by interpolating climatological grid coefficients of the GPT2 model according to the vessel's location and applying harmonic functions to account for seasonal variability. ZWD is computed as the difference between the total tropospheric delay and ZHD. Then, PWV can be written as

$$PWV = 10^6 \cdot \left[\rho \cdot R_w \cdot \left(\frac{3.739\times10^5}{T_m} + 22.1\right)\right]^{-1} \cdot ZWD \quad (2)$$

where ρ is the liquid water density, R_w represents the gas constant for water vapor, and T_m refers to the mean weighted temperature of the atmosphere (Davis et al., 1985; Bevis et al., 1994). The T_m is estimated using a linear relationship, $T_m = 70.2 + 0.72\, T_s$, with surface temperature T_s (Bevis et al., 1994). The T_s is obtained from the GPT2 model at the vessel's specified position.

3 Shipborne GNSS PWV

3.1 PWV at anchorage

Before evaluating the GNSS-derived PWV obtained from kinematic PPP in the ocean, we compare it with the PWVs calculated from nearby GNSS ground stations when the vessel is at anchor. In addition, a comparison of height variation using shipborne GNSS and a tide gauge operated by the Korea Hydrographic and Oceanographic Agency is also performed to validate the PPP method.

Figure 2a shows the distribution of the anchored R/V ISABU, two nearby GNSS ground stations, and a tide station. The separation distances between the anchored vessel and CHWN and GOSG stations are 27 and 34 km, respectively. And the distance from the tide gauge is 7 km. The shipborne and ground-based GNSS data and tide gauge data are used from DOY 209 to 210, immediately preceding the vessel's departure. Figure 2b illustrates the temporal variation in height of the vessel's

GNSS and tide gauge due to the sea level change over two days. Based on the 2-day time-series data, the GNSS height exhibits a mean of 48.8 m with a variation range of 1.4 m, whereas the tidal height averages 0.96 m with a range of 1.1 m. The range of height variation for both measurements is 1.1–1.4 meters. The change patterns are also similar. To evaluate the performance of PPP, the same epoch data sets are processed in an epoch-wise difference. After applying demean to both datasets, the RMS of the epoch-wise differences was calculated at 0.138 m. This allows us to validate the performance of PPP.

Figure 2c presents the PWV time series for two days. The data points were displayed only in 1-hour intervals for better visual clarity. The shipborne PWV from kinematic PPP shows good agreement, with the ground-based PWV derived from two stations, exhibiting a mean difference of 0.6–1.8 mm and an RMS of 2.1–2.9 mm. Meunram and Satirapod (2019) reported that as spatial correlation decreases, PWV variability increases, and the standard deviation also increases. Their result showed that the average standard deviation of PWV was approximately 2.2 mm when the distance between stations in the Thai region was set to within 20 km. A slight difference in this work can be attributed mainly to temperature and humidity differences, as well as the geographical location of the two regions (Rahman et al., 2025). Several studies have also demonstrated that the difference in PWV between the shipborne and ground-based datasets is less than 3 mm in terms of RMS (Bosser et al., 2021; Wu et al., 2022). Our results showed that the reliability of shipborne GNSS PWV was verified by comparing it with ground-based GNSS PWV.

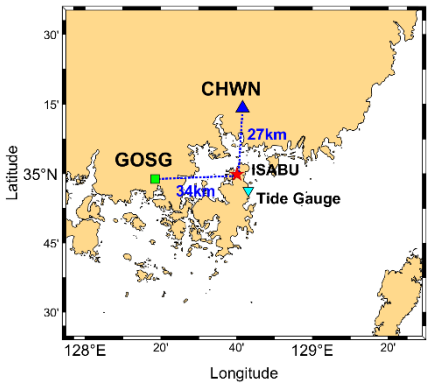

(a)

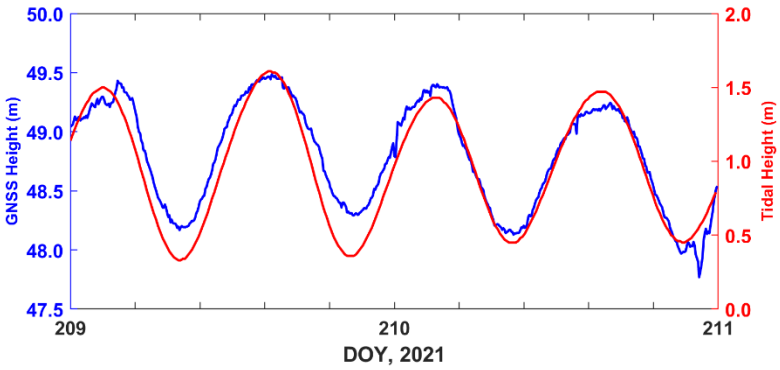

(b)

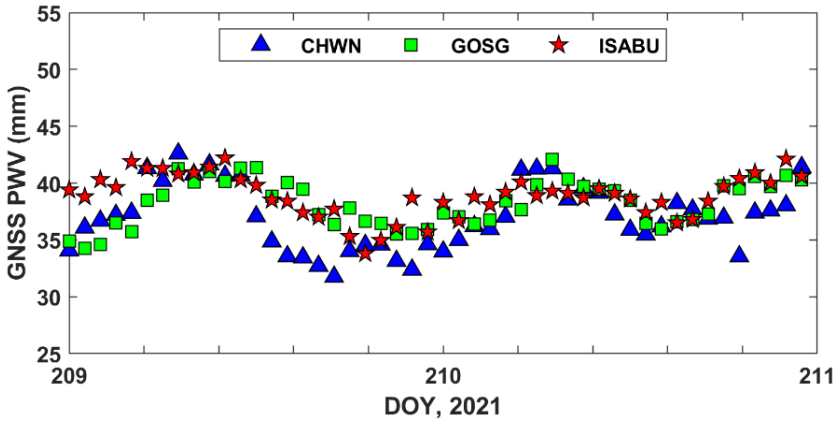

(c)

Figure 2. PWV from GNSS ground stations and R/V ISABU. (a) The distribution of two GNSS ground stations (CHWN and GOSG), R/V ISABU, and a tide station. (b) Height variation from the vessel's GNSS and tide gauge from DOY 209 to 210, 2021. (c) The time series of PWV was derived from the CHWN, GOSG, and R/V ISABU from DOY 209 to 210, 2021.

3.2 PWV time variation in the ocean

The R/V ISABU was operated for 27 days in the period DOY 211 through 237 to conduct marine science experiments. During this period, the vessel sailed from the Korean Peninsula to the Philippine Sea. The tropospheric precipitable water vapor was estimated along the path of the vessel movement.

Figure 3 shows the vessel trajectory with GNSS PWV during the campaign. The vessel departs on DOY 211 and sails south for about three days, arriving in the Philippine Sea on DOY 214 at about 21°N in latitude. It slowly moves toward the equator for about 17 days while the vessel moves between 126.5 and 133.5°E in longitude. On DOY 231, it turns in the Philippine Sea region at about 16°N in latitude and returns to heading north for about seven days. The R/V ISABU returned to its home port on DOY 237.

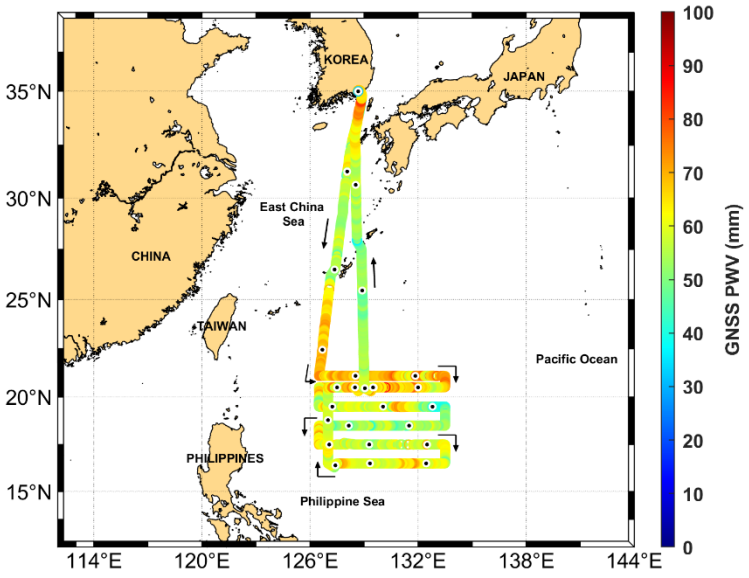

Figure 3. R/V ISABU trajectory with GNSS PWV for 27 days. The black dot on the white circle on the trajectory indicates the starting point of the day. The black arrows indicate the vessel's direction of travel.

The time series of shipborne GNSS PWV estimated at 5-minute intervals is shown in Fig. 4, as well as the count of PWV bins. The PWV values vary from 30 to 90 mm in range over the entire cruise. The estimated PWV range of 30–40 mm accounts for approximately 2.2%, 40–50 mm for 5.1%, 50–60 mm for 43.6%, 60–70 mm for 39.4%, and 70–80 mm for 9.5%. The measurement range of 50–60 mm has the highest occurrence count. Rivera et al. (2021) showed that the monthly mean variation of PWV in the northern Philippines area during the summer season (June-August) was 50–60 mm using radiosondes from 2012 to 2019. Our results tended to be in good agreement with Rivera's results.

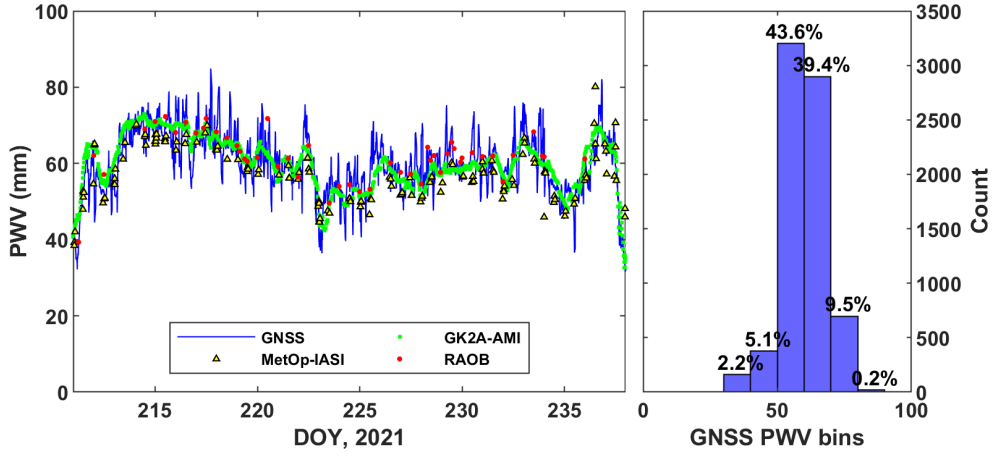

Figure 4. (Left) PWV time series for shipborne GNSS, radiosonde (RAOB), low Earth orbit (MetOp-IASI), and geostationary satellites (GK2A-AMI) for the 27 days from DOY 211 (July 30) to DOY 237 (August 25). (Right) Histogram for shipborne GNSS PWV count.

4 Results

4.1 Comparison to radiosonde observations

The shipborne GNSS PWV was evaluated using the ship-launched radiosonde observation (RAOB) profiles. Figure 5a shows a radiosonde balloon being launched from a vessel. The radiosonde model is the Vaisala RS41-SG, which is attached to a balloon and measures altitude, temperature, air pressure, relative humidity, dew point temperature, and winds vertically. The R/V ISABU had conducted 2–5 radiosonde observations per day over the ocean. These observations were made during the whole cruise (Fig. 4).

PWV can be calculated along the path of the sounding balloon as follows (Bock et al., 2005; Liu et al., 2013):

$$PWV = \frac{1}{g}\int_{P1}^{P2}\left(\frac{621.97e}{P-e}\right)dP \tag{3}$$

where g is the gravitational acceleration (g=9.80665 m/s^2); *P1* and *P2* are atmospheric pressure in the lower and upper layer (units: hPa); P is air pressure; and e is the actual water vapor pressure. Actual water vapor pressure can be computed from dew point temperature (T_d) in degrees Celsius using the equation derived from (Bolton, 1980):

$$e = 6.112 \times \exp\left(\frac{17.67\,T_d}{T_d+243.5}\right) \tag{4}$$

A typical radiosonde observation can last about two hours. We compared the shipborne GNSS PWV values with the ship-launched radiosonde at the radiosonde launching time. Wu et al. (2022) stated that the largest difference in RMS of PWV estimated at 30-minute time intervals from 30 to 120 minutes was only 0.2 mm, indicating that PWV values were relatively stable within 2 hours. In addition, a balloon can rise to approximately 30 km above the Earth's surface and drift more than 300 km from its release point. Although more than 99% of atmospheric water vapor is concentrated below approximately 10–15 km, PWV was calculated by integrating radiosonde measurements acquired during ascent to the maximum observation height. However, some of the received radiosonde observations are inaccurate due to signal loss. Such data can significantly affect the comparison of PWVs between two different observations. Therefore, we removed a few data points with a signal loss from the radiosonde.

The comparison between GNSS-derived PWV and radiosonde PWV is shown in Fig. 5b. The scatter plot shows a comparative analysis between GNSS PWV and RAOB PWV, and includes quantitative evaluations of the agreement between the two measurement methods. A total of 50 pairs are analysed. In the figure, the main statistical analysis results, including the linear relationship, correlation coefficient, mean, standard deviation (STD), and RMS error for the two datasets, are presented. The

linear regression indicated by the thick red line represents the best-fit relationship between the two variables. The red trend line is close to the black dotted reference line ($y = x$).

The mean bias is −0.94 mm, suggesting that GNSS PWV underestimates RAOB PWV on average by nearly 1 mm. The STD and RMS values of differences between the two datasets are 4.22 and 4.28 mm. These demonstrate that the GNSS method provides consistent and reasonably accurate measurements when compared to RAOB. Männel et al. (2021) reported a relatively smaller RMS of 1.47 kg m^{-2} in a comparison between the GNSS-based PWV and RS41 radiosonde observations, but conducted their experiments in the generally dry Arctic region.

The correlation coefficient generated by the Pearson correlation model is 0.80, indicating a very strong positive relationship between the two variables. While the two datasets exhibit substantial agreement, minor discrepancies are still present, likely attributable to differences in measurement techniques and temporal or spatial mismatches. The slope and intercept of the fitted line are 0.88 and 6.32, respectively. This reveals that GNSS PWV values are slightly underestimated compared to RAOB values, but there's a positive intercept, suggesting GNSS measurements start slightly higher overall.

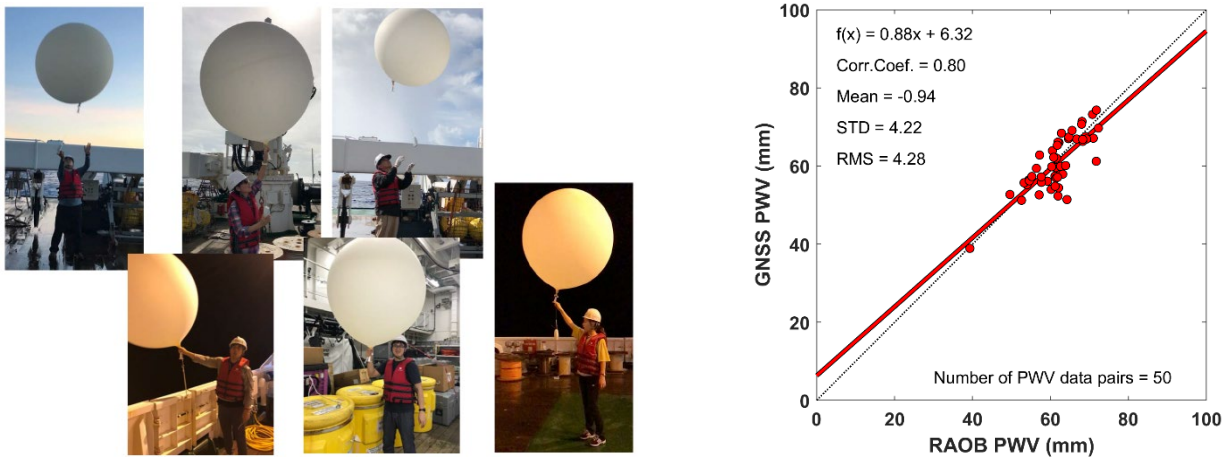

(a) (b)

Figure 5. Comparison of shipborne GNSS PWV against ship-launched radiosonde observations (RAOB) PWV. (a) Launching a radiosonde balloon on the vessel (Source: Kwon et al., 2019). (b) Scatter diagram of shipborne GNSS PWV and RAOB PWV. The legend displays the equation for a linear relationship, correlation coefficient, mean, standard deviation (STD), and root mean square (RMS) error. The thick red line and black dotted line represent the linear regression line and the reference line (y=x), respectively.

4.2 Comparison to satellite products

The shipborne GNSS PWV over the Pacific Ocean was also evaluated using satellite measurements. We used two different orbiting satellites: a geostationary satellite and a polar-orbiting satellite flying in low Earth orbit.

4.2.1 GNSS PWV vs GEO-KOMPSAT-2A-AMI PWV

The geostationary Korea multi-purpose satellite 2A (GEO-KOMPSAT-2A or GK2A) is a geostationary meteorological satellite operated by the National Meteorological Satellite Center (NMSC) of the Korea Meteorological Administration (KMA). The Advanced Meteorological Imager (AMI) on board the GK2A has a multi-channel capacity of 16 spectral channels, including 4 visible, 2 near-infrared, and 10 infrared channels (Kim et al., 2021). Its high spatial resolution is 0.5–1.0 km for visible and 2 km for infrared channels. It also enables fast full-disk imaging within 10 minutes and offers flexibility in regional area selection and scheduling. The GK2A-AMI has operationally provided 52 derived products that have been used to improve typhoon track and intensity forecasts, increase warning lead time for severe storms, improve detection of heavy rainfall and flash floods, and monitor a variety of other meteorological phenomena.

In this study, we used total precipitable water data, one of the secondary products. This dataset is extracted from NetCDF files provided by the web-based service (https://data.kma.go.kr/resources/html/en/aowdp.html). The GK2A-AMI captures the Earth's hemisphere every 10 minutes, but comparisons with GNSS PWV were performed at 30-minute intervals. As shown in Fig. 6a, satellite-borne PWV values were calculated using the average within ±0.5° of latitude and longitude from the vessel's location at the observation time. Wu et al. (2022) reported that a 100 km distance threshold could be taken as a reference threshold to validate shipborne GNSS PWV using satellite products. At this time, the number of satellite observation values within the target area was a minimum of 267, a maximum of 401, and an average of 350.

Figure 6b presents a scatter plot comparing PWV measurements derived from the GNSS receiver aboard the R/V ISABU with those obtained from the geostationary satellite GK2A-AMI. In this comparison, the GK2A-AMI-derived PWV values serve as the reference. A total of 1,225 pairs are analysed, as some data were not collected. The mean bias between the two datasets is calculated to be 0.08 mm, indicating a negligible systematic error. However, the STD and RMS are both 4.84 and 4.83 mm, suggesting the presence of moderate variability in the measurements. Taking the ground-based GNSS PWV compared with the PWV retrieval from geostationary satellite data showed an RMSE of approximately 2–5 mm (Wong et al., 2015; Du et al., 2024). Although the PWV correction due to the height difference between the GNSS antenna and sea level was not considered, the present results are reasonably consistent with previous studies.

The correlation coefficient between the two datasets is 0.79, reflecting a fairly strong positive linear relationship, although it is slightly lower than that observed with RAOB in the previous comparison. The green regression line represents the best-fit linear model, with a slope of 0.89 and an intercept of 6.88. The slope close to unity implies that the GNSS-derived PWV values are generally consistent with those from GK2A-AMI, though they exhibit slightly lower sensitivity. The positive intercept indicates a tendency for the GNSS measurements to slightly overestimate PWV at lower values.

Overall, the results demonstrate good agreement between the shipborne GNSS PWV and GK2A-AMI PWV, with minimal systematic bias and a strong linear relationship. The relatively wider dispersion of data points, compared to the GNSS–RAOB comparison, may be attributed to differences in satellite retrieval algorithms or atmospheric variability affecting the satellite observations.

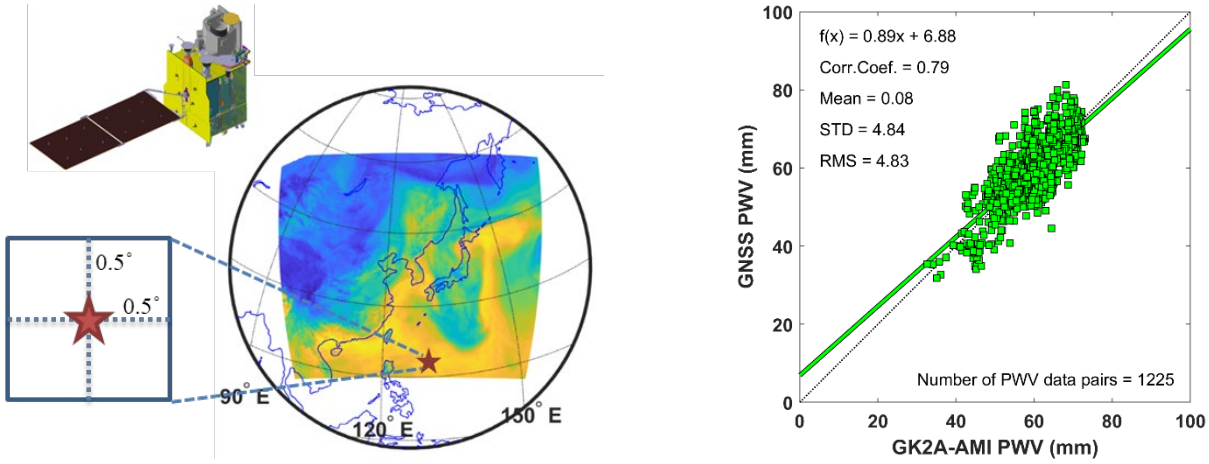

(a) (b)

Figure 6. Comparison of shipborne GNSS PWV against satellite GK2A-AMI PWV. (a) The satellite-borne PWV values were calculated using the average within ±0.5° of latitude and longitude from the vessel's location marked by a red star at the time of observation. (b) Scatter diagram of shipborne GNSS PWV and satellite GK2A-AMI PWV. The legend shows the equation for a linear relationship, correlation coefficient, mean, standard deviation (STD), and root mean square (RMS). The thick green line and black dotted line represent the linear regression line and the reference line ($y = x$), respectively. (Image source of the GK2A spacecraft: https://nmsc.kma.go.kr/enhome/html/base/cmm/selectPage.do?page=satellite.gk2a.operStatus)

4.2.2 GNSS PWV vs MetOp-IASI PWV

Low Earth Orbit (LEO) satellite data are widely used for water vapor monitoring due to their advantages, such as high-resolution imagery, reduced atmospheric interference, and fast data transmission, but their coverage is limited. The meteorological operational satellite programme (MetOp) is three (A, B, and C) polar-orbiting meteorological satellites operated by the European Organisation for the Exploitation of Meteorological Satellites (EUMETSAT). The MetOp satellites fly in at an altitude of approximately 817 km. They circle the sun synchronously 14.4 times a day and provide global observation data for weather forecasts and climate monitoring.

The infrared atmospheric sounding interferometer (IASI), one of the most important instruments onboard satellites, is a key payload of the MetOp satellite series. The IASI instrument is a nadir-viewing Fourier transform spectrometer. Its field of view consists of a 2 × 2 matrix of circular pixels with a 12 km diameter footprint on the ground at the nadir (Clerbaux et al., 2009). In this study, we used integrated water vapor data, one of the IASI level 2 products. This dataset is extracted from NetCDF format files provided by the website (https://user.eumetsat.int/data-access). As with the method previously compared to GK2A-AMI, IASI PWV values were averaged within ±0.5° of latitude and longitude from the vessel's position at the time of observation (Fig. 7a). The number of common observations between the two systems was 161 during the vessel journey. At

the common observation time, the number of satellite observation values within the target area was a minimum of 1, a maximum of 19, and an average of 11.

As shown in Fig. 7b, this scatter plot presents the relationship between PWV measurements retrieved from the R/V ISABU GNSS and those obtained from the MetOp-IASI satellite sensor. A total of 161 pairs are analysed. The linear regression line fitted to the data is expressed as $f(x) = 0.92x + 7.13$. The trend line has a slope of 0.92, which is closely aligned with the reference line ($y = x$), but suggests that GNSS PWV measurements have slightly lower sensitivity compared to MetOp-IASI estimates. The intercept of 7.13 mm indicates a tendency for GNSS to overestimate PWV at lower values.

The correlation coefficient of 0.71 reflects a strong linear relationship between the two datasets. This implies a reasonable level of agreement, though somewhat weaker than the correlation observed in previous comparisons with RAOB and GK2A-AMI. Using MetOp-IASI data as the reference, a mean bias of 2.58 mm suggests that GNSS measurements are generally higher than IASI values. Furthermore, an STD of 6.52 mm and an RMS of 6.99 mm reflect greater variability, likely influenced by differences in spatial resolution, sensing geometry, or atmospheric conditions affecting the satellite retrieval. These results are consistent with those of Bosser et al. (2021), who reported similar results when using LEO satellite data. They stated that the large RMS differences of 5–7 mm reflect enhanced uncertainties in LEO satellite products in tropical regions.

These results demonstrate that the agreement is weaker compared to other reference datasets, but the R/V ISABU GNSS-derived PWV shows a consistent relationship with MetOp-IASI measurements. This consistent relationship highlights its value as a complementary source for satellite-based PWV monitoring.

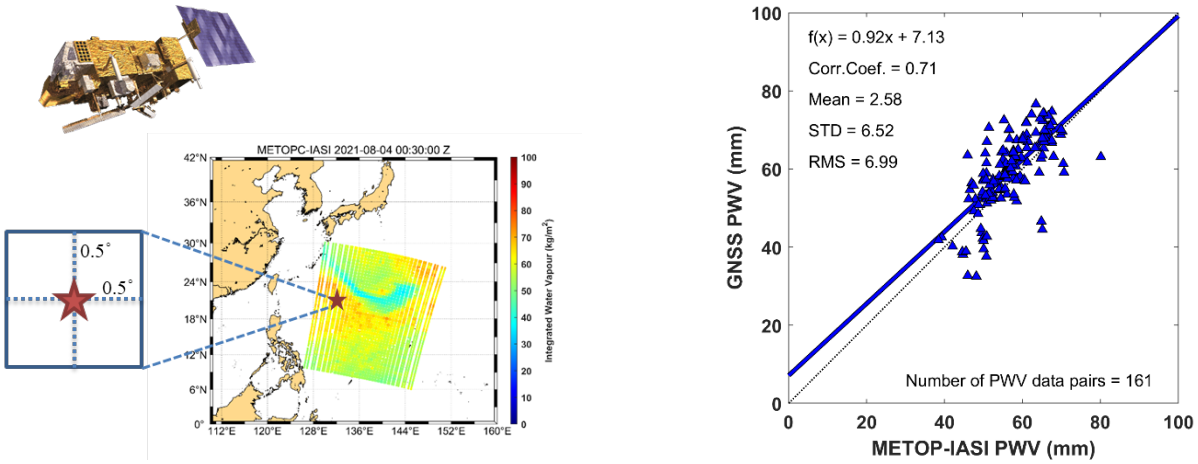

(a) (b)

Figure 7. Comparison of shipborne GNSS PWV against satellite MetOp-IASI PWV. (a) The satellite-borne PWV values were calculated using the average within ±0.5° of latitude and longitude from the vessel's location marked by a red star at the time of observation. (b) Scatter diagram of shipborne GNSS PWV and satellite MetOp-IASI PWV. The legend shows the equation for a linear relationship, correlation coefficient, mean, standard deviation (STD), and root mean square (RMS). The thick blue line and black dotted line represent the linear

regression line and the reference line (y=x), respectively. (Image source of MetOp spacecraft: https://www.eumetsat.int/our-satellites/metop-series)

5 Discussion

Figure 8 shows the time series for the shipborne GNSS PWV and rainfall rate from DOY 211 to 237 in 2021. The rainfall rate was derived using values observed from GK2A-AMI relative to the vessel's position (Fig. 6a). The shipborne GNSS PWV reveals a clear temporal pattern. At the beginning of the R/V journey, PWV values start relatively low, at approximately 35 mm. It increases sharply over the next few days, with PWV exceeding 70 mm around DOY 215. This abrupt rise is due to the vessel entering a tropical cyclone-prone region containing a strong influx of moisture as it moves toward lower latitudes. This phenomenon was expected because warm air can hold more water vapor than cold air. Figure 9 is a surface synoptic analysis weather map for Northeast Asia as of 00:00 UTC on DOY 214 (August 2, 2021). The weather map shows a tropical depression (TD) area forming in the western Philippine Sea, trapping a significant amount of water vapor in the atmosphere. At this time, the vessel was located at 22.45°N and 126.69°E (Fig. 9).

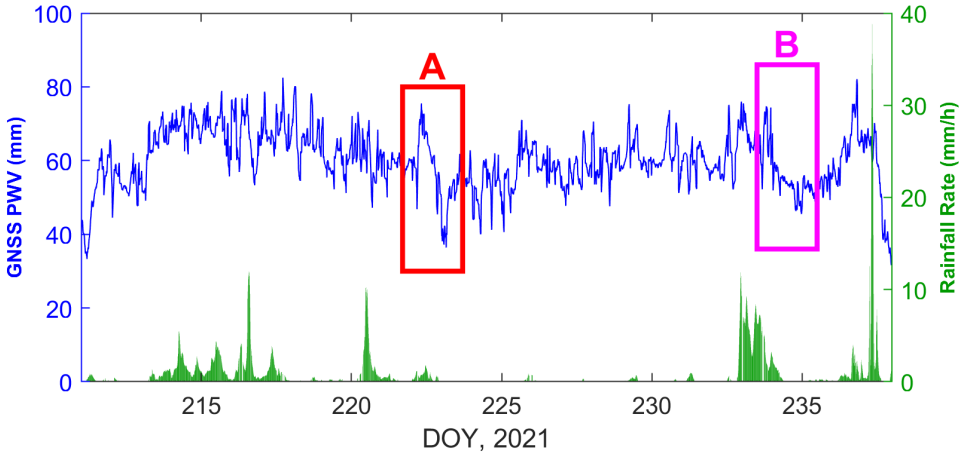

Figure 8. Time series for shipborne GNSS PWV and rainfall rate from DOY 211 to DOY 237. Boxes A and B represent periods of significant decline in PWV variation.

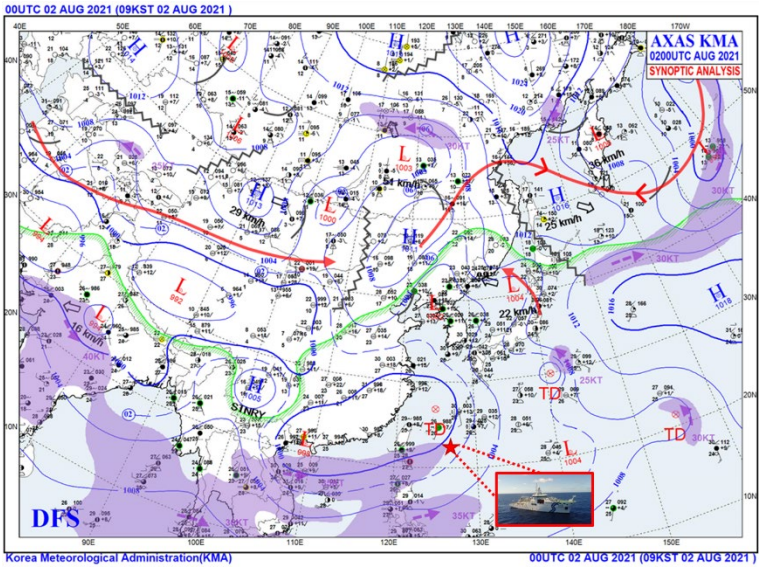

Figure 9. Surface synoptic analysis weather map for Northeast Asia at 00:00 UTC on DOY 214 (August 2, 2021) from the Korea Meteorological Administration (KMA). A tropical depression (TD) area is forming in the western Philippine Sea. The red star marks the vessel location at the time.

After that, from DOY 215 to 232, a value of PWV is generally maintained between 50 and 70 mm. However, as shown in the red rectangular A of Fig. 8, the PWV value rapidly decreases from 76 mm to less than 40 mm on DOY 222 (August 10, 2021). As shown in Fig. 8, there is rainfall before this period. Figure 10 presents the weather forecast chart for mean sea level pressure and accumulated precipitation at 12:00 UTC on DOY 222. At this time, the vessel was located at 19.50°N and 131.42°E (Fig. 10). The synoptic chart indicates the presence of precipitation at the vessel's location. This precipitation area exhibits a northward progression along the pressure trough, transitioning from lower to mid-latitudes. This phenomenon indicates that a strong rainfall event led to the rapid condensation of atmospheric water vapor, resulting in a steep decrease in PWV (Barindelli et al., 2018; Sapucci et al., 2019; Gopalan et al., 2021).

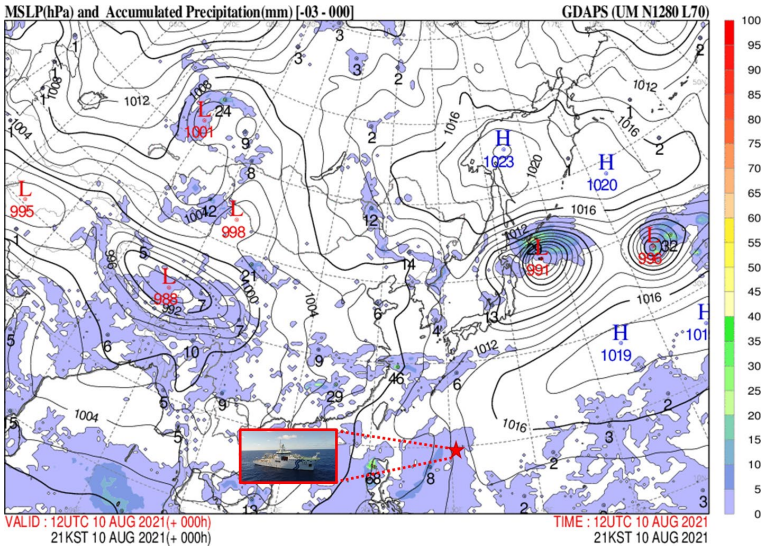

Figure 10. Weather forecast chart for mean sea level pressure (MSLP) and accumulated precipitation from the Korea Meteorological Administration (KMA) at 12:00 UTC on DOY 222 (August 10, 2021). The red star marks the vessel location at the time.

After DOY 233, the variability in PWV increases again, with some sharp drops and rises occurring repeatedly. During this period, unstable trends are observed, such as PWV falling below 50 mm or rising above 80 mm. Particularly around DOY 233–236, the time series exhibits large amplitude fluctuations, potentially indicating localized precipitation events or abrupt meteorological changes. As shown in the magenta rectangular B of Fig. 8, on DOY 234 (August 22, 2021), GNSS PWV decreases from 75 mm to about 45 mm. The figure also shows that the rainfall occurs before the PWV decreases. At 12:00 UTC on this day, the R/V ISABU is located at 22.88°N and 128.97°E and moves north toward the Korean Peninsula (Fig. 11). Typhoon OMAIS, which developed over the sea approximately 850 km south-southeast of Okinawa, Japan, is propagating northeastward along the periphery of the subtropical high-pressure system. The R/V returns to its home port following Typhoon OMAIS. As mentioned earlier, GNSS PWV decreased after a typhoon with heavy rainfall passed (Song and Grejner-Brzezinska, 2009; Chen et al., 2021). Zhao et al. (2019) observed that PWV exhibits a marked increase in association with the approach of a typhoon, followed by a gradual decrease as the storm moves away. In addition, the movement of the vessel from low to mid-latitudes also affects the decrease in PWV, as shown in the final part of the time series in the Fig. 8.

In our PPP processing strategy, we utilized the GPT2 model rather than in-situ measurements to ensure continuous and stable kinematic positioning by avoiding potential sensor anomalies. However, it should be noted that relying on the meteorological model can introduce biases in the estimated PWV. This is particularly relevant during cyclonic events, where significant pressure anomalies could result in a PWV bias.

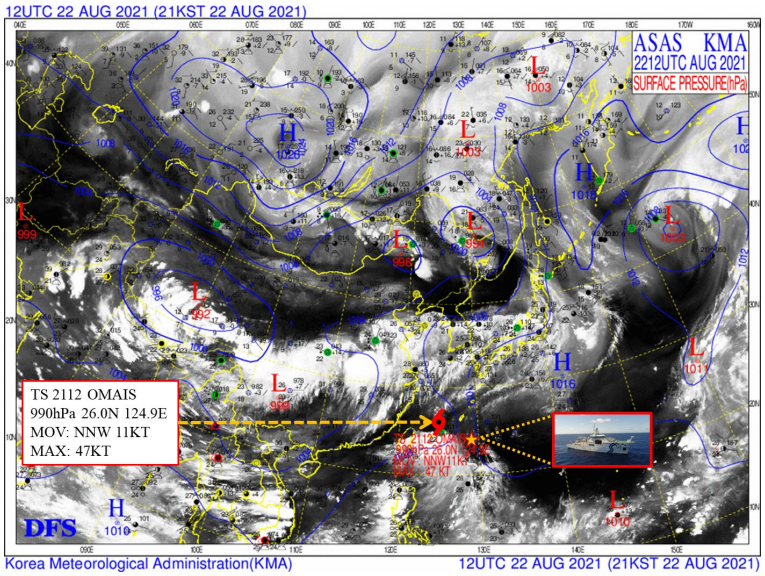

385 **Figure 11.** Weather forecast chart from Korea Meteorological Administration (KMA) at 12:00 UTC on DOY 234 (August 22, 2021). An orange star with a red border marks the vessel location at the time. Typhoon OMAIS, which originated in the sea about 850 km south-southeast of Okinawa, Japan, is moving northeast along the edge of the subtropical high pressure (KMA, 2022).

6 Conclusion

In this study, we presented the retrieval of PWV from shipborne multi-GNSS measurements conducted on the R/V ISABU
390 during the summer in tropical cyclone-prone regions of the Northwest Pacific following the previous study. Validation of the GNSS-derived PWV against radiosonde, geostationary orbit (GK2A-AMI), and low Earth orbit (MetOp-IASI) observations confirmed its reliability for monitoring atmospheric water vapor over oceanic regions. We showed that reliable results can be obtained for the shipborne GNSS PWV over the ocean by using observations from similar regions at different times and comparing them with another dataset. Furthermore, we showed that decreases in GNSS-derived PWV are closely associated
395 with precipitation, which also includes rainfall related to tropical cyclone activity.

The GNSS PWV showed good agreement with RAOB measurements, characterized by a mean bias of −0.94 mm, an RMS of 4.28 mm, and a correlation coefficient of 0.80, indicating high consistency and low systematic error. Comparison with GK2A-AMI PWV also yielded a negligible bias of 0.08 mm, an RMS of 4.83 mm, and a correlation coefficient of 0.79. In contrast, the MetOp-IASI observations exhibit a larger mean bias of 2.58 mm and greater dispersion with an RMS of 6.99 mm, likely
400 due to differences in spatial resolution, sensing geometry, and retrieval algorithms. Despite the relatively large RMS value, a correlation coefficient of 0.71 indicates a strong linear relationship and thus reflects a reasonable level of agreement between the two datasets. In the previous study, shipborne GNSS-PWV showed an RMS of 5.22 mm and 8.97 mm compared to radiosonde and low Earth orbit (Aqua-AIRS), respectively (Sohn et al., 2020). The GNSS-derived PWV obtained from a

moving vessel shows consistent performance across multiple reference datasets. This consistency supports its utility as a complementary and reliable data source for atmospheric water vapor estimation in both research and operational applications. While observations over oceanic and terrestrial surfaces may have a relatively limited direct impact on numerical weather prediction models, they remain essential for accurately defining the lower boundary conditions of atmospheric modeling (Saunders, 2021). Although this work estimated the amount of water vapor using a single specific receiver, as the number of vessels equipped with GNSS receivers capable of recording raw observation data continues to increase and data-sharing systems further develop, the availability of shipborne GNSS PWV data is expected to improve. Consequently, such data are anticipated to play a growing role in weather forecasting and climate research, particularly in oceanic regions where other observations remain sparse. In addition, PWV retrieved from shipborne GNSS observations can be used to calibrate or validate satellite water vapor measurements.

Data availability.

The shipborne GNSS datasets used in this study are available from the corresponding author upon reasonable request. The GNSS datasets on the Korean Peninsula are available on the GNSS DATA CENTER (http://www.gnssdata.or.kr/main/getMainView.do, last access: 7 May 2024). The GK2A-AMI dataset is extracted from NetCDF files provided by the NMSC data provision service (https://data.kma.go.kr/resources/html/en/aowdp.html, last access: 28 August 2022). The MetOp-IASI dataset can be provided by the data centre (https://user.eumetsat.int/data-access/, last access: 25 March 2023).

Author contributions.

DS, BC, JH, YP, and JC carried out the conceptualization; DS, BC, JH, and BL processed the shipborne GNSS, GK2A-AMI, and MetOp-IASI data; YP and HJ provided the radiosonde data; DS, BC, and YP conducted the formal analysis and wrote the original draft; DS and BC completed the review and edited the manuscript. All authors have read and approved the final version of the manuscript.

Competing interests.

The authors declare that they have no conflict of interest.

Acknowledgements

We thank all crews of the R/V ISABU of the KIOST for their assistance during the GNSS installation, operations, and data archiving. We would like to thank Mr. Chan-Ki Jeong for his help in using the weather forecast chart. Finally, we appreciate the anonymous reviewers for their assistance in evaluating this paper and their helpful comments.

Financial support

This work was supported by the National Research Foundation of Korea (NRF) grant funded by the Korean government (Ministry of Science and ICT) (No.2021R1C1C2008774). This work was also partly supported by the basic research fund from the Korea Astronomy and Space Science Institute (No.2026-1-8-5300). This research was also partly supported by the Korea Institute of Marine Science & Technology Promotion (KIMST) funded by the Ministry of Oceans and Fisheries (RS-2022-KS221667).

Review statement

This paper was edited by Roeland Van Malderen and reviewed by two anonymous referees.

References

Barindelli, S., Realini, E., Venuti, G., Fermi, A., and Gatti, A.: Detection of water vapor time variations associated with heavy rain in northern Italy by geodetic and low-cost GNSS receivers, Earth Planets Space, 70, 28, doi:10.1186/s40623-018-0795-7, 2018.

Bevis, M., Businger, S., Herring, T. A., Rocken, C., Anthes, R. A., and Ware, R. H.: GPS Meteorology: Remote sensing of atmospheric water vapor using the global positioning system, J. Geophys. Res., 97, 15787–15801, doi:10.1029/92JD01517, 1992.

Bevis, M., Businger, S., Chiswell, S., Herring, T. A., Anthes, R. A., Rocken, C., and Ware, R. H.: GPS Meteorology: Mapping Zenith Wet Delays onto Precipitable Water, J. Appl. Meteorol., 33, 379–386, doi:10.1175/1520-0450(1994)033<0379:GMMZWD>2.0.CO;2, 1994.

Bock, O., Keil, C., Richard, E., Flamant, C., and Bouin, M.: Validation of precipitable water from ECMWF model analyses with GPS and radiosonde data during the MAP SOP, Q. J. R. Meteorol. Soc., 131, 3013–3036, doi:10.1256/qj.05.27, 2005.

Boehm, J., Niell, A., Tregoning, P., and Schuh, H.: Global Mapping Function (GMF): A new empirical mapping function based on numerical weather model data, Geophys. Res. Lett., 33, L07304, doi:10.1029/2005GL025546, 2006.

Bolton, D.: The Computation of Equivalent Potential Temperature, Monthly Weather Review, 108, 1046–1053, doi:10.1175/1520-0493(1980)108<1046:TCOEPT>2.0.CO;2, 1980.

Boniface, K., Champollion, C., Chery, J., Ducrocq, V., Rocken, C., Doerflinger, E., and Collard, P.: Potential of shipborne GPS atmospheric delay data for prediction of Mediterranean intense weather events, Atmos. Sci. Lett., 13, 250–256, doi:10.1002/asl.391, 2012.

Bosser, P., Bock, O., Flamant, C., Bony, S., and Speich, S.: Integrated water vapour content retrievals from ship-borne GNSS receivers during EUREC4A, Earth Syst. Sci. Data, 13, 1499–1517, doi:10.5194/essd-13-1499-2021, 2021.

Bosser, P., Van Baelen, J., and Bousquet, O.: Routine Measurement of Water Vapour Using GNSS in the Framework of the Map-Io Project, Atmosphere, 13, 903, doi:10.3390/atmos13060903, 2022.

Chen, J., Mai, C., Zhou, M., Chen, S., Li, W., Fang, R., and Zhao, Z.: Influence of water vapor distribution on the simulated track of Typhoon Hato (2017), Nat. Hazards, 109, 2363–2380, doi:10.1007/s11069-021-04923-2, 2021.

Choi, B.-K., Roh, K.-M., Cho, S.-K., Park, J.-U., Park, P.-H., and Lee, S. J.: Development of the Kinematic Global Positioning System Precise Point Positioning Method Using 3-Pass Filter, Journal of Astronomy and Space Sciences, 29, 269–274, doi:10.5140/JASS.2012.29.3.269, 2012.

Choi, B.-K., Cho, C.-H., and Lee, S. J.: Multi-GNSS Kinematic Precise Point Positioning: Some Results in South Korea, Journal of Positioning, Navigation, and Timing, 6, 35–41, doi:10.11003/JPNT.2017.6.1.35, 2017.

Choi, B.-K. and Yoon, H.: Positioning stability improvement with inter-system biases on multi-GNSS PPP, Journal of Applied Geodesy, 12, 239–248, doi:10.1515/jag-2018-0005, 2018.

Clerbaux, C., Boynard, A., Clarisse, L., George, M., Hadji-Lazaro, J., Herbin, H., Hurtmans, D., Pommier, M., Razavi, A., Turquety, S., Wespes, C., and Coheur, P.-F.: Monitoring of atmospheric composition using the thermal infrared IASI/MetOp sounder, Atmos. Chem. Phys., 9, 6041–6054, doi:10.5194/acp-9-6041-2009, 2009.

Davis, J. L., Herring, T. A., Shapiro, I. I., Rogers, A. E. E., and Elgered, G.: Geodesy by radio interferometry: Effects of atmospheric modeling errors on estimates of baseline length, Radio. Sci., 20, 1593–1607, doi:10.1029/RS020i006p01593, 1985.

Deng, Z., Fritsche, M., Nischan, T., and Bradke, M.: Multi-GNSS Ultra Rapid Orbit-, Clock- & EOP-Product Series. GFZ Data Services. doi:10.5880/GFZ.1.1.2016.003, 2016.

Du, Z., Yao, Y., Zhang, B., and Zhao, Q.: Precipitable water vapor estimation from Himawari-8/AHI observations using a stacking machine learning model, Atmospheric Research, 301, 107281, doi:10.1016/j.atmosres.2024.107281, 2024.

Elgered, G., Davis, J. L., Herring, T. A., and Shapiro, I. I.: Geodesy by radio interferometry: Water vapor radiometry for estimation of the wet delay, J. Geophys. Res., 96, 6541–6555, doi:10.1029/90JB00834, 1991.

Fan, S. J., Zang, J. F., Peng, X. Y., Wu, S. Q., Liu, Y. X., and Zhang, K. F.: Validation of atmospheric water vapor derived from ship-borne GPS measurements in the Chinese Bohai Sea, Terr. Atmos. Ocean. Sci., 27, 213–220, doi: 10.3319/TAO.2015.11.04.01(A), 2016.

Fujita, M., Kimura, F., Yoneyama, K., and Yoshizaki, M.: Verification of precipitable water vapor estimated from shipborne GPS measurements, Geophys. Res. Lett., 35, L13803, doi:10.1029/2008GL033764, 2008.

Gopalan, K., Shukla, B. P., Sharma, S., Kumar, P., Shyam, A., Gaur, A., and Sunda, S.: An Observational Study of GPS-Derived Integrated Water Vapor over India, Atmosphere, 12, 1303, doi:10.3390/atmos12101303, 2021.

He, H., Yang, J., Wu, L., Gong, D., Wang, B., and Gao, M.: Unusual growth in intense typhoon occurrences over the Philippine Sea in September after the mid-2000s, Clim. Dyn. 48, 1893–1910, doi:10.1007/s00382-016-3181-9, 2017.

He, J., and Liu, Z.: Water Vapor Retrieval from MODIS NIR Channels Using Ground-Based GPS Data, IEEE Trans. Geosci. Remote Sens., 58, 3726–3737, doi:10.1109/TGRS.2019.2962057, 2020.

Ikuta, Y., Seko, H., and Shoji, Y.: Assimilation of shipborne precipitable water vapour by Global Navigation Satellite Systems for extreme precipitation events, Quarterly Journal of the Royal Meteorological Society, 148, 57–75, doi:10.1002/qj.4192, 2022.

IGS (International GNSS Service), Global network of IGS stations, [Internet], viewed 2025 Jun 21, available from: https://network.igs.org/, 2025.

JMA (Japan Meteorological Agency): 2021 Annual report on the activities of the RSMC Tokyo Typhoon Center, 2022.

Kang, S. K., Kim, S.-H., Lin, I.-I., Park, Y.-H., Choi, Y., Ginis, I., Cione, J., Shin, J. Y., Kim, E. J., Kim, K. O., Kang, H. W., Park, J.-H., Bidlot, J.-R., and Ward, B.: The North Equatorial Current and rapid intensification of super typhoons, Nat. Commun., 15, 1742, doi:10.1038/s41467-024-45685-2, 2024.

Kealy, J., Foster, J., and Businger, S.: GPS meteorology: An investigation of ocean-based precipitable water estimates, J. Geophys. Res., 117, D17303, doi:10.1029/2011JD017422, 2012.

Kim, D., Gu, M., Oh, T.-H., Kim, E.-K., and Yang, H.-J.: Introduction of the Advanced Meteorological Imager of Geo-Kompsat-2a: In-Orbit Tests and Performance Validation, Remote Sens., 13, 1303, doi:10.3390/rs13071303, 2021.

KMA (Korea Meteorological Administration), 2021 Annual typhoon analysis report (in Korean), 2022.

Kwon, M., Lee, D.-W., Lee, K.-J., Kim, S.-Y., and Lee, J.-H.: Radiosonde observations in the western North Pacific area, 4th Year of Maritime Continent meeting, 2019.

Lagler, K., Schindelegger, M., Boehm, J., Krásná, H., and Nilsson, T.: GPT2: Empirical slant delay model for radio space geodetic techniques, Geophys. Res. Lett., 40, 1069–1073, doi:10.1002/grl.50288, 2013.

Liu, Y., Liu, Y., Chen, G., and Wu, Z.: Evaluation of HY-2A satellite-borne water vapor radiometer with shipborne GPS and GLONASS observations over the Indian Ocean, GPS Solut., 23, 87, doi:10.1007/s10291-019-0876-5, 2019.

Liu, Z., Wong, M. S., Nichol, J., and Chan, P. W.: A multi-sensor study of water vapour from radiosonde, MODIS and AERONET: a case study of Hong Kong, Int. J. Climatol., 33, 109–120, doi:10.1002/joc.3412, 2013.

Männel, B., Zus, F., Dick, G., Glaser, S., Semmling, M., Balidakis, K., Wickert, J., Maturilli, M., Dahlke, S., and Schuh, H.: GNSS-based water vapor estimation and validation during the MOSAiC expedition, Atmos. Meas. Tech., 14, 5127–5138, doi:10.5194/amt-14-5127-2021, 2021.

Meunram, P., and Satirapod, C.: Spatial variation of precipitable water vapor derived from GNSS CORS in Thailand, Geodesy and Geodynamics, 10, 140–145, doi:10.1016/j.geog.2019.01.003, 2019.

Niell, A. E., Coster, A. J., Solheim, F. S., Mendes, V. B., Toor, P. C., Langley, R. B., and Upham, C. A.: Comparison of Measurements of Atmospheric Wet Delay by Radiosonde, Water Vapor Radiometer, GPS, and VLBI, J. Atmos. Ocean. Technol., 18, 830–850, doi:10.1175/1520-0426(2001)018<0830:COMOAW>2.0.CO;2, 2001.

Panetier, A., Bosser, P., and Khenchaf, A.: Sensitivity of Shipborne GNSS Troposphere Retrieval to Processing Parameters. In: International Association of Geodesy Symposia. Springer, Berlin, Heidelberg, doi:10.1007/1345_2022_177, 2022.

Park, J. K., Kim, B. S., Jung, W. S., Kim, E. B., and Lee, D. G.: Change in Statistical Characteristics of Typhoon Affecting the Korean Peninsula, Atmosphere, 16, 1–17 (in Korean), 2006.

Rahman, G., Kim, J. Y., Kim, T. W., Park, M., and Kwon, H. H.: Spatial and temporal variations in temperature and precipitation trends in South Korea over the past half-century (1974–2023) using innovative trend analysis, Journal of Hydro-environment Research, 58, 1–18, doi:10.1016/j.jher.2024.11.002, 2025.

Rivera, Y., Capacete, K. C., Rodriguez, S. K., David, A. R., and Macalalad, E.: Variations of precipitable water vapor from 2012 to 2019 over the Philippines using radiosondes, IOP Conf. Ser. Earth Environ. Sci., 880, 012001, IOP Publishing, doi:10.1088/1755-1315/880/1/012001, 2021.

Rocken, C., Johnson, J., Hove, T. V., and Iwabuchi, T.: Atmospheric water vapor and geoid measurements in the open ocean with GPS, Geophys. Res. Lett., 32, L12813, doi:10.1029/2005GL022573, 2005.

Saastamoinen, J.: Contributions to the theory of atmospheric refraction: Part II. Refraction corrections in satellite geodesy, Bulletin Géodésique, 107, 13–34, doi:10.1007/BF02522083, 1973.

Saunders, R.: The use of satellite data in numerical weather prediction, Weather, 76, 95–97, doi:10.1002/wea.3913, 2021.

Sapucci, L. F., Machado, L. A., de Souza, E. M., and Campos, T. B.: Global Positioning System precipitable water vapour (GPS-PWV) jumps before intense rain events: A potential application to nowcasting, Meteorol. Appl., 26, 49–63, doi:10.1002/met.1735, 2019.

Shoji, Y., Sato, K., and Yabuki, M.: Comparison of shipborne GNSS-derived precipitable water vapor with radiosonde in the western North Pacific and in the seas adjacent to Japan, Earth Planets Space, 69, 153, doi:10.1186/s40623-017-0740-1, 2017.

Smith, S. R., Alory, G., Andersson, A., Asher, W., Baker, A., Berry, D. I., Drushka, K., Figurskey, D., Freeman, E., Holthus, P., Jickells, T., Kleta, H., Kent, E. C., Kolodziejczyk, N., Kramp, M., Loh, Z., Poli, P., Schuster, U., Steventon, E., Swart, S., Tarasova, O., de la Villeon, L. P., Vinogradova-Shiffer, N.: Ship-Based Contributions to Global Ocean, Weather, and Climate Observing Systems, Front. Mar. Sci., 6, 434, doi:10.3389/fmars.2019.00434, 2019.

Sohn, D.-H., Choi, B.-K., Park, Y., Kim, Y. C., and Ku, B.: Precipitable Water Vapor Retrieval from Shipborne GNSS Observations on the Korean Research Vessel ISABU, Sensors, 20(15), 4261. doi:10.3390/s20154261, 2020.

Song, D. S., and Grejner-Brzezinska, D. A.: Remote sensing of atmospheric water vapor variation from GPS measurements during a severe weather event, Earth Planet Sp., 61, 1117–1125, doi:10.1186/BF03352964, 2009.

Wang, J., and Zhang, L.: Systematic Errors in Global Radiosonde Precipitable Water Data from Comparisons with Ground-Based GPS Measurements, J. Clim., 21, 2218–2238, doi:10.1175/2007JCLI1944.1, 2008.

Wang, J., Wu, Z., Semmling, M., Zus, F., Gerland, S., Ramatschi, M., Ge, M., Wickert, J., and Schuh, H.: Retrieving Precipitable Water Vapor From Shipborne Multi-GNSS Observations, Geophysical Research Letters, 46, doi:10.1029/2019GL082136, 2019.

Wong, M. S., Jin, X., Liu, Z., Nichol, J. E., Ye, S., Jiang, P., and Chan, P. W.: Geostationary Satellite Observation of Precipitable Water Vapor Using an Empirical Orthogonal Function (EOF) based Reconstruction Technique over Eastern China, Remote Sens., 7, 5879–5900, doi:10.3390/rs70505879, 2015.

Wu, J. T., Wu, S. C., Hajj, G. A., Bertiger, W. I., and Lichten, S. M.: Effects of antenna orientation on GPS carrier phase, Manuscr. Geod., 18, 91–98, doi:10.1007/BF03655303, 1993.

Wu, Z., Liu, Y., Liu, Y., Wang, J., He, X., Xu, W., Ge, M., and Schuh, H.: Validating HY-2A CMR precipitable water vapor using ground-based and shipborne GNSS observations, Atmos. Meas. Tech., 13, 4963–4972, doi:10.5194/amt-13-4963-2020, 2020.

Wu, Z., Lu, C., Zheng, Y., Liu, Y., Liu, Y., Xu, W., Ke, J., and Tang, Q.: Evaluation of Shipborne GNSS Precipitable Water Vapor Over Global Oceans From 2014 to 2018, IEEE Transactions on Geoscience and Remote Sensing, 60, 1–15, doi:10.1109/TGRS.2022.3142745, 2022.

Zhao, Q., Ma, X., Yao, W., and Yao, Y.: A New Typhoon-Monitoring Method Using Precipitation Water Vapor, Remote Sensing, 11(23), 2845, doi:10.3390/rs11232845, 2019.